DTU Library

An analytical model of flagellate hydrodynamics

Dölger, Julia; Bohr, Tomas; Andersen, Anders Peter

Link back to DTU Orbit

An analytical model of flagellate hydrodynamics

Julia Dölger, Tomas Bohr, and Anders Andersen[*]

Department of Physics and Centre for Ocean Life, Technical University of Denmark,
DK-2800 Kgs. Lyngby, Denmark

[*]Correspondence and requests for materials should be addressed to A.A. (email:
aanders@fysik.dtu.dk).

Abstract. Flagellates are unicellular microswimmers that propel themselves using one or several beating flagella. We consider a hydrodynamic model of flagellates and explore the effect of flagellar arrangement and beat pattern on swimming kinematics and near-cell flow. The model is based on the analytical solution by Oseen for the low Reynolds number flow due to a point force outside a no-slip sphere. The no-slip sphere represents the cell and the point force a single flagellum. By superposition we are able to model a freely swimming flagellate with several flagella. For biflagellates with left-right symmetric flagellar arrangements we determine the swimming velocity, and we show that transversal forces due to the periodic movements of the flagella can promote swimming. For a model flagellate with both a longitudinal and a transversal flagellum we determine radius and pitch of the helical swimming trajectory. We find that the longitudinal flagellum is responsible for the average translational motion whereas the transversal flagellum governs the rotational motion. Finally, we show that the transversal flagellum can lead to strong feeding currents to localized capture sites on the cell surface.

Submitted to: *Phys. Scr.*

1. Introduction

Unicellular plankton play an essential role in aquatic ecosystems and their survival functions depend crucially on their flow environment and the flows that they generate [Guasto et al., 2012, Pécseli et al., 2014]. The flow fields due to freely swimming plankton contain information on the extent of flow disturbances that attract flow sensing predators, feeding currents that enhance prey capture and nutrient uptake, and the power at which energy is dissipated in the water [Guasto et al., 2012, Kiørboe, 2016]. Many unicellular organisms use flagella (actuated filaments) to swim [Gibbons, 1981, Fenchel, 1986]. The bacterium *Escherichia coli* and the algae *Chlamydomonas reinhardtii* have been investigated extensively as representatives of flagellated microswimmers [Berg, 2008, Goldstein, 2015, Lauga, 2016]. However, those two model organisms do not represent the diversity of flagellar arrangements and beat patterns of the large group of flagellated microswimmers in the aquatic environment [Lighthill, 1976, Sleigh, 1981, Inouye and Hori, 1991].

In this article we present a hydrodynamic model of eukaryotic flagellates with focus on swimming kinematics and near-cell flows (figure 1). It is largely unknown, what the flagellar characteristics are optimized for and which strategies and functions they reflect. Our model has the potential to address these questions. The Reynolds number that gives the ratio between inertial and viscous forces is much less than unity for microswimmers [Purcell, 1977]. Flagellate hydrodynamics is therefore governed by the time-independent Stokes equation and the equation of continuity for incompressible flows

$$\nabla p \quad = \mu \nabla^2 \mathbf{v} \; , \tag{1}$$

$$\nabla \cdot \mathbf{v} = 0 \; , \tag{2}$$

where p is the pressure, $\mathbf{v}$ the flow velocity, and μ the dynamic viscosity. Both analytical and numerical models have been developed to study such creeping flows.

Point force models based on the Stokeslet, i.e., the fundamental Green's function solution of the creeping flow due to a single point force, are able to represent the far field around different microswimmers [Lauga and Powers, 2009, Drescher et al., 2010, Drescher et al., 2011, Pak and Lauga, 2016]. A neutrally buoyant microswimmer experiences negligible net force and torque. The most basic point force model of freely swimming microorganisms is thus the stresslet that models two counteracting forces that act on the water and are related to the thrust due to the swimming appendages and the drag on the body, respectively [Lauga and Powers, 2009]. The stresslet represents the far field around *E. coli* [Drescher et al., 2011]. A model consisting of three point forces has successfully been used for biflagellates with two left-right symmetric flagella, and it represents well the main flow patterns around *C. reinhardtii* [Drescher et al., 2010]. With this model the far field decay of flow disturbances has been studied and equatorial force arrangements were shown to be the most "quiet", i.e., leading to the least flow disturbances [Kiørboe et al., 2014, Andersen et al., 2015].

However, point force models completely disregard the presence of the cell, which is
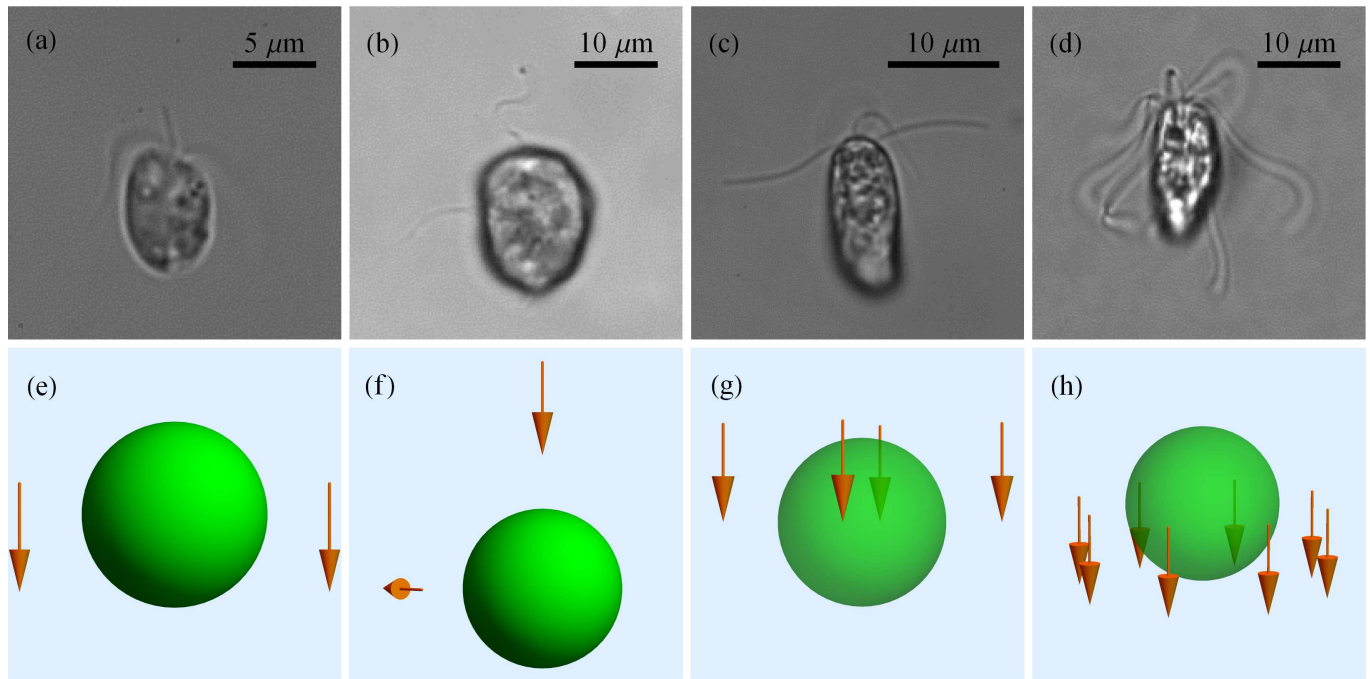
Figure 1. Flagellates with different flagellar arrangements and beat patterns. (a)-(d) Microscope images of freely swimming individuals. (e)-(h) Model descriptions with vectors (orange) indicating the flagellar forces on the water. (a) and (e): *Prymnesium parvum*, a left-right symmetric biflagellate (haptophyte) with a haptonema at the front. (b) and (f): *Heterosigma akashiwo* with a longitudinal (puller) flagellum and a transversal flagellum. (c) and (g): *Tetraselmis sp.* with two pairs of flagella that beat in anti-phase. (d) and (h): *Pyramimonas octopus* with eight flagella. The microscope images are shown by courtesy of Lasse Tor Nielsen.

essential for the study of swimming kinematics and near-cell flows. One model that can be used for such studies is the squirmer model of ciliates covered with cilia that create a net flow close to the cell surface [Lighthill, 1952, Blake, 1971, Pak and Lauga, 2016]. However, other types of models that take the hydrodynamic interaction between flagella and cell into account are needed to describe swimming kinematics and near-cell flows in flagellates [Kurtuldu et al., 2013, Polotzek and Friedrich, 2013]. An analytical three-sphere model has been used, e.g., to study flagellar synchronization and swimming kinematics in biflagellates [Friedrich and Jülicher, 2012, Polotzek and Friedrich, 2013]. Another possible approach for representing near fields is to build on the solution derived by Oseen for the flow due to a point force in proximity of a sphere with no-slip boundary [Oseen, 1927, Pozrikidis, 1992]. This solution forms the basis of analytical models that have been used to describe freely swimming copepods [Jiang et al., 2002] and to investigate the swimming and feeding of uniflagellates [Higdon, 1979a, Higdon, 1979b, Langlois et al., 2009]. Such a model for freely swimming biflagellates with two left-right symmetric forces was also recently used to represent near-cell flows around biflagellated haptophytes with focus on swimming and feeding [Dölger et al., 2017]. Also for computational fluid dynamics models of flagellated microswimmers a similar

flow solution with regularized Stokeslets next to a sphere has been proven to be useful [Wrobel et al., 2016].

We here establish a general analytical model of freely swimming flagellates, which is based on the Oseen solution and has the potential to represent swimming kinematics and near-cell flows. We present the basic building block giving the flow for an arbitrary point force representing one flagellum of a freely swimming spherical cell. The flow field of a flagellate propelled by several flagella can be obtained by linear flow superposition of such basic flows. As illustrative examples we consider a flagellate with two left-right symmetric forces that by construction swims on a straight path (figures 1(a) and 1(e)) and a flagellate propelled by two point forces that produce a helical trajectory (figures 1(b) and 1(f)). For the different cases we show how swimming characteristics and flow properties depend on flagellar arrangement and beat pattern.

2. General model framework

The basic building block of the flagellate model is the flow around a freely translating and rotating sphere propelled by a single point force (figure 2(a)). To establish the model we build on the solution by Oseen for the creeping flow due to a point force $\mathbf{F}$ that is acting on the water in proximity of a fixed no-slip sphere [Oseen, 1927, Pozrikidis, 1992]. The flow field can be written

$$v_{\mathrm{O},j}(\mathbf{x}) = \frac{1}{8\pi\mu} G_{jk}(\mathbf{x}, \mathbf{X}) F_k , \tag{3}$$

where the Green's function G_{jk} depends on the field vector $\mathbf{x}$ and the point force location $\mathbf{X}$ (Appendix A). The flow created by the point force results in a force $\mathbf{K}$ and a torque $\mathbf{L}$ on the sphere that depend on the radial force component $\mathbf{F}_{\mathrm{r}} = (\mathbf{F} \cdot \mathbf{X})\mathbf{X}/R^2$, the tangential force component $\mathbf{F}_{\mathrm{t}} = \mathbf{F} - \mathbf{F}_{\mathrm{r}}$, and the force distance $R = |\mathbf{X}|$, i.e.,

$$\mathbf{K} = \frac{1}{2}\left[\frac{3}{R/a} - \frac{1}{(R/a)^3}\right]\mathbf{F}_{\mathrm{r}} + \frac{1}{4}\left[\frac{3}{R/a} + \frac{1}{(R/a)^3}\right]\mathbf{F}_{\mathrm{t}} , \tag{4}$$

$$\mathbf{L} = \frac{1}{(R/a)^3}\mathbf{X} \times \mathbf{F} , \tag{5}$$

where a is the radius of the sphere [Pozrikidis, 1992, equations (3.3.26) and (3.3.27)]. Equations (4) and (5) can be derived using the Faxén relations and the Stokeslet flow solution in an infinite domain without knowledge of the flow solution (3).

If the model flagellate is free to translate and rotate, the net force and torque on it in the creeping flow are zero. We assume a rigid and frictionless connection between the sphere and the point where the force is produced, so that the thrust force $\mathbf{T} = -\mathbf{F}$ is transferred directly to the cell (figure 2(a)). At equilibrium there is balance between the thrust force $\mathbf{T}$, the force $\mathbf{K}$, and the drag $\mathbf{D} = -6\pi\mu a\mathbf{U}$ due to the translational motion of the sphere, and thus its velocity $\mathbf{U}$ is determined by

$$\begin{aligned} 6\,\pi\,\mu\,a\,\mathbf{U} &= \mathbf{T} + \mathbf{K} \\ &= f_1(R/a)\,\mathbf{T} + f_2(R/a)\,\frac{(\mathbf{X} \cdot \mathbf{T})\,\mathbf{X}}{R^2} . \end{aligned} \tag{6}$$
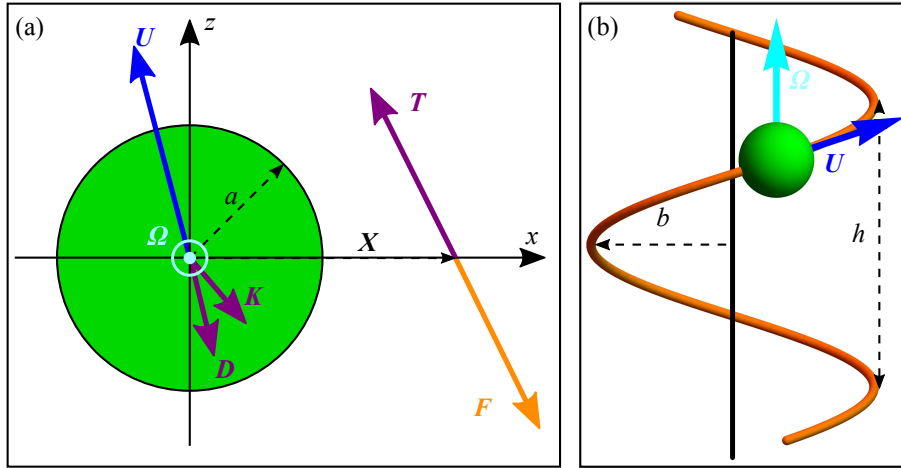
Figure 2. Flagellate model and swimming kinematics. (a) Basic building block with one point force. Sphere (green), point force $\mathbf{F}$ acting on the fluid (orange), forces acting on the organism (purple), i.e., the thrust force $\mathbf{T}$, the force $\mathbf{K}$ due to the flow produced by the point force, and the Stokes drag $\mathbf{D} = -6\,\pi\,\mu\,a\,\mathbf{U}$ due to the translational motion with velocity $\mathbf{U}$ (blue). The angular velocity $\mathbf{\Omega}$ (light blue) is directed out of the plane in the negative y-direction. (b) Helical trajectory with radius b and pitch h for a sphere translating with velocity $\mathbf{U}$ and rotating with angular velocity $\mathbf{\Omega}$ due to several point forces.

Similarly there is balance between the torque $\mathbf{X} \times \mathbf{T}$ due to the thrust force $\mathbf{T}$, the torque $\mathbf{L}$, and the resistive torque $\mathbf{M} = -8\pi\mu a^3 \mathbf{\Omega}$ on the sphere due to its rotational motion, and thus the angular velocity $\mathbf{\Omega}$ is determined by

$$8\,\pi\,\mu\,a^3\,\mathbf{\Omega} = \mathbf{X} \times \mathbf{T} + \mathbf{L}$$
$$= f_3(R/a)\,\mathbf{X} \times \mathbf{T} \, . \tag{7}$$

The dimensionless coefficients f_1, f_2, and f_3 depend only on the dimensionless force distance R/a and they turn out to be

$$f_1 = 1 - \frac{3}{4\,R/a} - \frac{1}{4\,(R/a)^3} \, , \tag{8}$$

$$f_2 = -\frac{3}{4\,R/a} + \frac{3}{4\,(R/a)^3} \, , \tag{9}$$

$$f_3 = 1 - \frac{1}{(R/a)^3} \, . \tag{10}$$

To model flagellates with several flagella or several thrust force locations per flagellum, each flow solution representing one point force $\mathbf{F}_i$ at position $\mathbf{X}_i$ can be calculated separately from equation (3) and superposed with the flow fields due to the forces created by the other flagella to obtain the total flow $\mathbf{v}_\mathrm{O} = \sum_i \mathbf{v}_{\mathrm{O},i}$. The translational and the angular velocity can be obtained by superposition of the velocities due to each flagellum, i.e., $\mathbf{U} = \sum_i \mathbf{U}_i$ and $\mathbf{\Omega} = \sum_i \mathbf{\Omega}_i$.
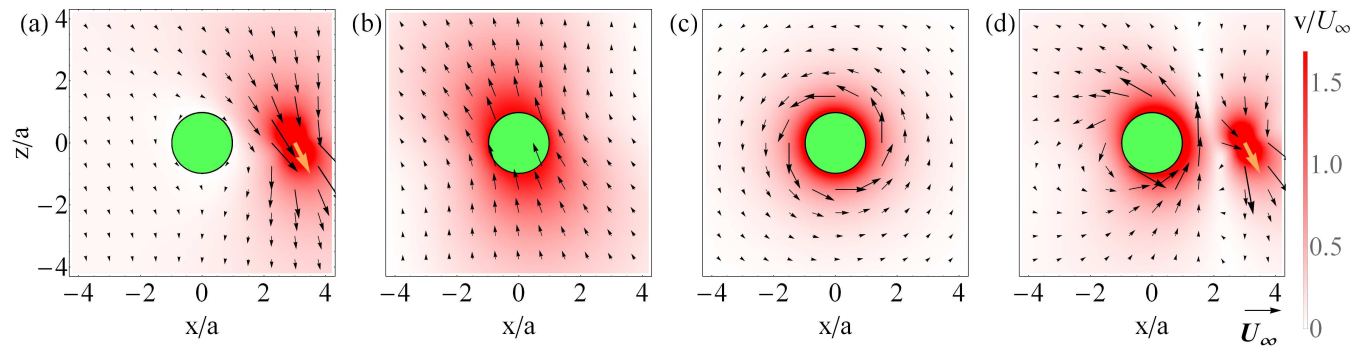
Figure 3. Superposition of creeping flows to calculate the flow around a freely swimming model flagellate. (a) Flow due to a point force (vector, orange) outside a sphere. (b) Flow due to a translating sphere. (c) Flow due to a rotating sphere. (d) Superposition of the flows shown in (a)-(c) resulting in the flow around the freely swimming model flagellate. The colour maps show the normalized velocity magnitude v/U_∞ with the velocity scale $U_\infty = F/(6\,\pi\,\mu\,a)$.

To calculate the flow around the freely swimming model organism [Jiang et al., 2002], the Oseen solution $\mathbf{v}_\mathrm{O}$ is superposed with the flow

$$\mathbf{v}_\mathrm{T} = \left[\frac{3}{4\,r/a} + \frac{1}{4\,(r/a)^3}\right]\mathbf{U} + \left[\frac{3}{4\,r/a} - \frac{3}{4\,(r/a)^3}\right]\frac{(\mathbf{x}\cdot\mathbf{U})\,\mathbf{x}}{r^2} \tag{11}$$

due to translation with velocity $\mathbf{U}$ and the flow

$$\mathbf{v}_\mathrm{R} = \frac{1}{(r/a)^3}\,\boldsymbol{\Omega}\times\mathbf{x} \tag{12}$$

due to rotation with angular velocity $\boldsymbol{\Omega}$ [Stone and Duprat, 2016]. The complete velocity field becomes

$$\mathbf{v} = \mathbf{v}_\mathrm{O} + \mathbf{v}_\mathrm{T} + \mathbf{v}_\mathrm{R}. \tag{13}$$

Superposition of the three flow field contributions leads in general to a complex flow field with both translational and rotational components near the cell and intense singular flow in the vicinity of the point force (figure 3).

3. Straight, circular, and helical trajectories

The vectors $\mathbf{U}$ and $\boldsymbol{\Omega}$ together determine the trajectory of the microswimmer. A model flagellate propelled by a single constant point force swims in the symmetry plane spanned by $\mathbf{X}$ and $\mathbf{T}$. Formally, looking at the expressions (6) and (7) and using that $\mathbf{X}\times\mathbf{T}$ is perpendicular to the plane spanned by $\mathbf{X}$ and $\mathbf{T}$, we see that $\mathbf{U}$ is perpendicular to $\boldsymbol{\Omega}$. The trajectory is thus in this case restricted to a circle, or a straight line when $\boldsymbol{\Omega} = \mathbf{0}$.

For a general model flagellate propelled by several constant point forces, $\mathbf{U}$ and $\boldsymbol{\Omega}$ are neither parallel nor perpendicular to each other and the swimming trajectory is helical (figure 2(b)). The velocity $\mathbf{U}$ is constant in the co-rotating coordinate system

with axes that follow the rotation of the microswimmer, and without loss of generality we define $\mathbf{e}_z = \mathbf{\Omega}/\Omega$ and decompose $\mathbf{U} = U_\perp \mathbf{e}_y + U_\parallel \mathbf{e}_z$ with

$$U_\parallel = \mathbf{U} \cdot \mathbf{e}_z , \tag{14}$$

$$U_\perp = \sqrt{U^2 - (\mathbf{U} \cdot \mathbf{e}_z)^2} . \tag{15}$$

The velocity $\mathbf{U}'$ of the cell center in the stationary coordinate system with axes that are fixed is calculated by rotating the velocity vector $\mathbf{U}$ around the z-axis as

$$\begin{bmatrix} U_{x'} \\ U_{y'} \\ U_{z'} \end{bmatrix} = \begin{bmatrix} \cos\Omega t & -\sin\Omega t & 0 \\ \sin\Omega t & \cos\Omega t & 0 \\ 0 & 0 & 1 \end{bmatrix} \begin{bmatrix} 0 \\ U_\perp \\ U_\parallel \end{bmatrix} . \tag{16}$$

Integration yields the trajectory $\mathbf{s}'(t)$ of the cell center in the stationary coordinate system as

$$\mathbf{s}'(t) = \int \mathbf{U}' \mathrm{d}t = \frac{U_\perp}{\Omega} \left(\cos\Omega t \, \mathbf{e}_{x'} + \sin\Omega t \, \mathbf{e}_{y'} \right) + U_\parallel t \, \mathbf{e}_{z'} , \tag{17}$$

which describes a helical trajectory around the z'-axis (figure 2(b)). We can identify the helix radius

$$b = \frac{U_\perp}{\Omega} \tag{18}$$

and the pitch

$$h = \frac{2\pi U_\parallel}{\Omega} . \tag{19}$$

For constant $\mathbf{U}$ and $\mathbf{\Omega}$ the orientation of the flagellate is constant with respect to the locally defined Frenet-Serret basis for the helical trajectory such that some points on the cell surface are always on the "outside" and some on the "inside" of the trajectory [Crenshaw, 1993a].

4. Flagellate propelled by two left-right symmetric forces

As a special case we look at a left-right symmetric model flagellate propelled by two constant point forces. This model can represent common biflagellates such as *C. reinhardtii* and some species of haptophytes such as *Prymnesium parvum* (figures 1(a) and 1(e)) [Dölger et al., 2017]. The two point forces $\mathbf{F}_1$ and $\mathbf{F}_2$ of equal magnitude F are assumed to lie in the xz-plane with radial and angular force positions R and θ, and force direction α (figure 4(a)).

Since the transversal force components towards and away from the symmetry axis cancel due to the left-right symmetry, the swimming velocity will point along the symmetry axis. Also, the torques due to the two point forces fully cancel each other and thus the model microswimmer does not rotate. The thrust force $\mathbf{T} = 2F \cos\alpha \, \mathbf{e}_z$ is proportional to the force components along the symmetry axis. As function of force
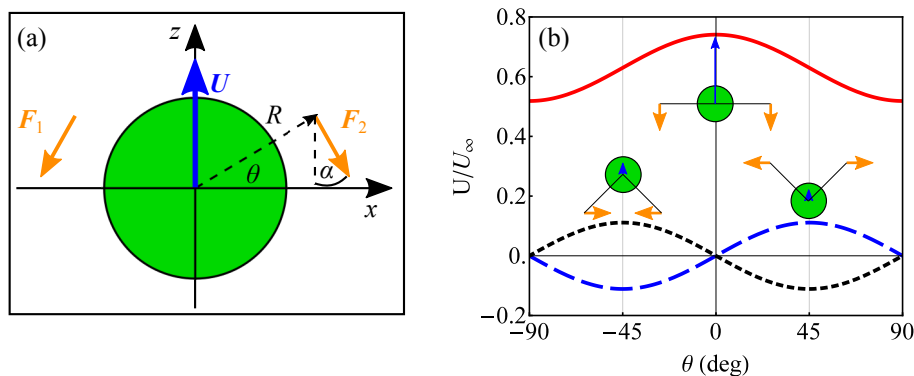
Figure 4. Model and swimming velocity for a left-right symmetric biflagellate. (a) Model microswimmer with fixed point forces $\mathbf{F}_1$ and $\mathbf{F}_2$ (orange) and translational velocity $\mathbf{U}$ (blue). Radial and angular force positions R and θ, and force direction α. (b) Normalized swimming velocity in the z-direction for the force distance $R = 3\,a$ as function of the angular force position θ for backwards pointing forces, i.e., $\alpha = 0$ (red line, solid) and transversely directed forces with $\alpha = 90\,\mathrm{deg}$ (blue line, dashed) and $\alpha = 270\,\mathrm{deg}$ (black line, dotted). The swimming velocity is maximal for equatorially placed, backwards pointing forces.

position and orientation the swimming velocity can be calculated using equation (6) as

$$\frac{U}{U_\infty} = \cos\alpha\left[1 - \frac{3\left(1 + \sin^2\theta\right)}{4\,R/a} - \frac{1 - 3\sin^2\theta}{4\left(R/a\right)^3}\right]$$

$$+ \frac{3}{8}\sin\alpha\,\sin 2\theta\left[\frac{1}{R/a} - \frac{1}{(R/a)^3}\right]\,, \tag{20}$$

where

$$U_\infty = \frac{F}{3\,\pi\,\mu\,a}\,. \tag{21}$$

The highest swimming velocity U_∞ is obtained when the forces are pointing backwards ($\alpha = 0$) and are placed far away from the cell. In this case the model reduces to that of a towed sphere. With a fixed point force magnitude F and distance R, the fastest swimming is obtained for an equatorial force arrangement with $\theta = 0$ and $\alpha = 0$ (figure 4(b)). The biflagellated haptophyte *P. parvum* has a cell radius of $a = 3\,\mu\mathrm{m}$ and an average swimming speed of $U = 30\,\mu\mathrm{m\,s^{-1}}$ [Dölger et al., 2017]. Using equation (20) for forces with $R = 8\,\mu\mathrm{m}$, $\theta = 0$, and $\alpha = 0$ we estimate that $U = 0.7\,U_\infty$, and using equation (21) with $\mu = 1 \cdot 10^{-3}\,\mathrm{Pa\,s}$ we find that each flagellum of *P. parvum* exerts an average force of $F = 1\,\mathrm{pN}$ on the water. A model swimmer with the above-mentioned force configuration produces a flow field that compares well with the measured time-averaged flow field around the biflagellate *P. parvum* [Dölger et al., 2017]. Our force estimate is comparable to the estimated average force per flagellum of approximately 5 pN for the larger *C. reinhardtii* [Drescher et al., 2010, Goldstein, 2015].

So far we have looked at models for steady microswimmers with constant point forces that represent time-averaged flow fields. In reality the periodic shape change of the beating flagella leads to periodically varying forces on the water [Purcell, 1977].
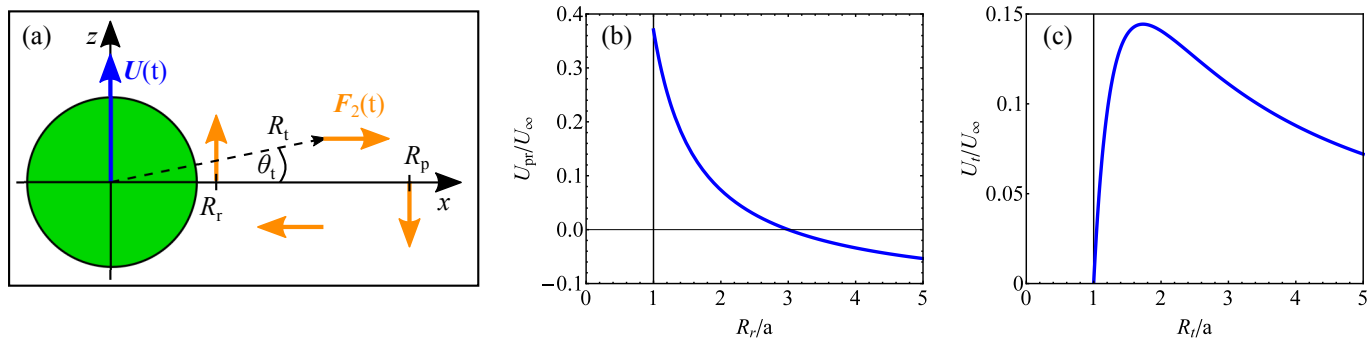
Figure 5. Time-dependent model and normalized swimming velocity for a left-right symmetric biflagellate. (a) Right half of model microswimmer with point force $\mathbf{F}_2(t)$ varying during the beat cycle. Forces for power and return strokes are placed equatorially, i.e., $\theta_\mathrm{p} = \theta_\mathrm{r} = 0$ with radial positions R_p and R_r. The transversal forces are placed symmetrically at $\pm\theta_\mathrm{t}$ with radial position R_t. (b) Average swimming velocity in the z-direction due to power and return stroke as function of return stroke distance R_r/a for $R_\mathrm{p} = 3\,a$ and $\theta_\mathrm{p} = 0$. (c) Average swimming velocity in the z-direction due to transversal strokes as function of transversal force distance R_t/a for $\theta_\mathrm{t} = \theta_\mathrm{opt} = 45\,\mathrm{deg}$. The swimming velocity is highest for return strokes close to the cell and transversal strokes with radial position $R_\mathrm{t} = R_\mathrm{opt} = \sqrt{3}\,a$.

If the point forces simply rotate at fixed locations relative to the cell and the time-average of each point force vanishes, there is no net propulsion. However, if the forces additionally move on closed trajectories relative to the cell, the model organism can swim due to the drag difference between different force positions. This mechanism of force variation can model the breast-stroke beat of biflagellates with short flagella, and has been shown to capture measured time-resolved near-cell flow fields around *P. parvum* [Dölger et al., 2017]. Here we ask which periodic force variation leads to the highest average swimming velocity, and what the effect is of the transversal forces.

As a schematic model we approximate the breast-stroke beat by four pairs of point forces of constant magnitude F that each act during one fourth of the beat period (figure 5(a)). The optimal angular arrangement for the power stroke is according to equation (20) at the equator at $\theta_\mathrm{p} = 0$. The further away from the cell the power stroke acts, the faster the model organism swims. Thus we assume that the distance R_p of the power stroke is set by the flagella length to a maximum feasible value. The return stroke is assumed to be positioned at the equator as well with $\theta_\mathrm{r} = 0$. It will lead to propulsion in the opposite direction to the power stroke. The velocity contribution due to the power and the return stroke is then calculated as

$$\frac{U_\mathrm{pr}}{U_\infty} = \frac{1}{8}\left[\frac{3}{R_\mathrm{r}/a} - \frac{3}{R_\mathrm{p}/a} + \frac{1}{(R_\mathrm{r}/a)^3} - \frac{1}{(R_\mathrm{p}/a)^3}\right], \qquad (22)$$

which is positive for $R_\mathrm{r} < R_\mathrm{p}$ (figure 5(b)). Also the purely transversal forces can lead to propulsion due to the force $\mathbf{K}$ when located below or above the equator, although their direct thrust $\mathbf{T}_1 + \mathbf{T}_2 = \mathbf{0}$ vanishes. The transversal forces are assumed to be symmetrically arranged at $\pm\theta_\mathrm{t}$ and at equal distance R_t. They both lead to swimming

in the positive z-direction with the velocity contribution

$$\frac{U_{\mathrm{t}}}{U_\infty} = \frac{3}{8} \sin 2\,\theta_{\mathrm{t}} \left[\frac{1}{R_{\mathrm{t}}/a} - \frac{1}{(R_{\mathrm{t}}/a)^3} \right] . \tag{23}$$

For any force distance R_{t} the highest velocity can be obtained for transversal forces located at the angular positions $\pm\theta_{\mathrm{opt}} = \pm 45\,\mathrm{deg}$. The optimum distance of the transversal forces is $R_{\mathrm{opt}} = \sqrt{3}\,a$ (figure 5(c)), so that the maximum velocity that can be obtained from the transversal forces is $U_{\mathrm{t}}(R_{\mathrm{opt}}, \theta_{\mathrm{opt}}) = 0.14\,U_\infty$. Correspondingly for a combined power and return stroke in an equatorial arrangement with $R_{\mathrm{p}} = 3\,a$ and $R_{\mathrm{r}} = 1.1\,a$ we find the swimming velocity $U_{\mathrm{pr}} = 0.30\,U_\infty$, and we conclude that the transversal forces can contribute significantly to facilitate swimming in biflagellates.

5. Simple flagellate model with helical trajectory

With more than one constant point force a model flagellate generally swims with a helical trajectory if the forces are not symmetrically arranged to create straight or circular trajectories. Helical trajectories are common among flagellates [Fenchel, 2001, Jennings, 1901, Jennings, 1904], and they are useful for helical klinotaxis, i.e., the movement towards stimuli due to gradients (chemical, light, temperature, magnetic field) [Crenshaw, 1993b, Crenshaw, 1996, Friedrich and Jülicher, 2009]. Here we study a flagellate with a longitudinal flagellum that creates a typical puller arrangement with a force $\mathbf{F}_1 = -F_1\,\mathbf{e}_z$ at $\mathbf{X}_1 = R\,\mathbf{e}_z$, and a transversal flagellum that creates a force tangentially to the surface of the sphere $\mathbf{F}_2 = -F_2\,\mathbf{e}_y$ at $\mathbf{X}_2 = R\,\mathbf{e}_x$ (figure 6(a)). The flagellate *Heterosigma akashiwo* has a flagellar arrangement for which this model can be applied (figures 1(b) and 1(f)). For simplicity we only explore the effect of the y-component of the force due to the transversal flagellum, and we disregard possible force components in other directions. Such components are most likely also created by the transversal flagellum of *H. akashiwo*.

The translational velocity is calculated with equation (6) as

$$6\,\pi\,\mu\,a\,\mathbf{U} = f_1\,F_2\,\mathbf{e}_y + (f_1 + f_2)\,F_1\,\mathbf{e}_z \tag{24}$$

and the angular velocity with equation (7) as

$$8\,\pi\,\mu\,a^3\,\boldsymbol{\Omega} = f_3\,R\,F_2\,\mathbf{e}_z . \tag{25}$$

In the resulting helical trajectory the longitudinal force $\mathbf{F}_1$ will always be directed parallel to the helix axis, while the transversal force $\mathbf{F}_2$ will always be positioned on the outside of the helix. The velocity component $U_\parallel$, see equation (14), due to the longitudinal force $\mathbf{F}_1$ leads to forward motion

$$U_\parallel = \frac{(f_1 + f_2)\,F_1}{6\,\pi\,\mu\,a} , \tag{26}$$

while the component $U_\perp$, see equation (15), due to the transversal force $\mathbf{F}_2$ leads to the rotational motion in the helix

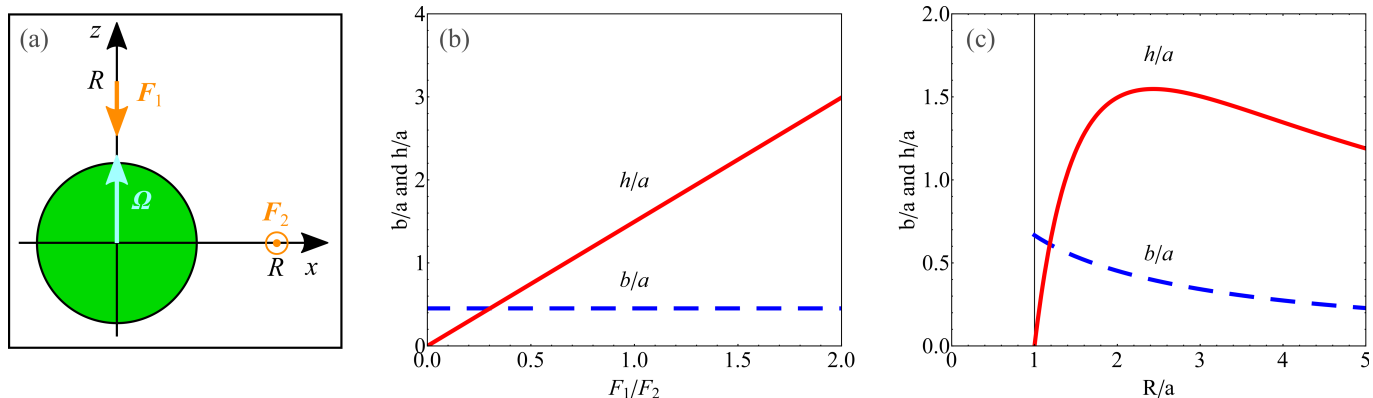$$U_\perp = \frac{f_1\,F_2}{6\,\pi\,\mu\,a} . \tag{27}$$

Figure 6. Model flagellate with helical trajectory. (a) Model microswimmer with point forces $\mathbf{F}_1$ and $\mathbf{F}_2$ (orange) and angular velocity $\boldsymbol{\Omega}$ (light blue). (b) and (c) Helix radius b/a (dashed line, blue) and helix pitch h/a (solid line, red) as functions of the force ratio F_1/F_2 for $R = 2\,a$ (b) and as functions of the force distance R/a for $F_1 = F_2$ (c). The radius decreases for increasing force distance from a maximum $b = b_{\max} = (2/3)\,a$. The pitch increases linearly with the force ratio F_1/F_2 and has a maximum at a force distance of $R = R_{\mathrm{opt}} \approx 2.4\,a$.

Thus for a constant longitudinal force $\mathbf{F}_1$ leading to a constant average translational velocity, the shape of the helical trajectory can be tuned by varying the magnitude of the tangential force $\mathbf{F}_2$. The radius is independent of the force ratio F_1/F_2 and depends only on the force distance. It is calculated with equation (18) as

$$\frac{b}{a} = \frac{1 + R/a + 4\,(R/a)^2}{3\,[R/a + (R/a)^2 + (R/a)^3]} \ . \tag{28}$$

The pitch also depends on the force distance and it is proportional to the force ratio F_1/F_2. It can be written using equation (19) as

$$\frac{h}{a} = 4\,\pi\,\frac{-1 - R/a + 2\,(R/a)^2}{3\,[R/a + (R/a)^2 + (R/a)^3]}\,\frac{F_1}{F_2} \ . \tag{29}$$

The dependences of the pitch and the radius on the force distance R/a and the force ratio F_1/F_2 show several characteristic features (figures 6(b) and 6(c)). The radius decreases with force distance from its maximum value $b_{\max} = (2/3)\,a$ to zero at large force distances, while the pitch first increases from zero to a maximum $h_{\max} \approx 1.5\,(F_1/F_2)\,a$ for the force distance $R_{\mathrm{opt}} \approx 2.4\,a$, and subsequently decreases as $(R/a)^{-1}$ for large R/a. A typical individual of *H. akashiwo* with a cell radius of $a = 5\,\mu\mathrm{m}$ swims with $U_\parallel = 50\,\mu\mathrm{m\,s}^{-1}$, $U_\perp = 90\,\mu\mathrm{m\,s}^{-1}$, and $\Omega = 2\,\mathrm{s}^{-1}$ [Gurarie et al., 2011]. From equations (18) and (19) we estimate $b = 40\,\mu\mathrm{m}$ and $h = 160\,\mu\mathrm{m}$. The large radius ($b > (2/3)\,a$) indicates that the transversal flagellum does not only produce a tangential force in the y-direction but also a radial force in the x-direction that allows larger radii of circular motion than in our simplified configuration.

The near-cell flow field can be used to find the optimal place for prey capture on the cell where the clearance rate per unit surface area is highest (figure 7)
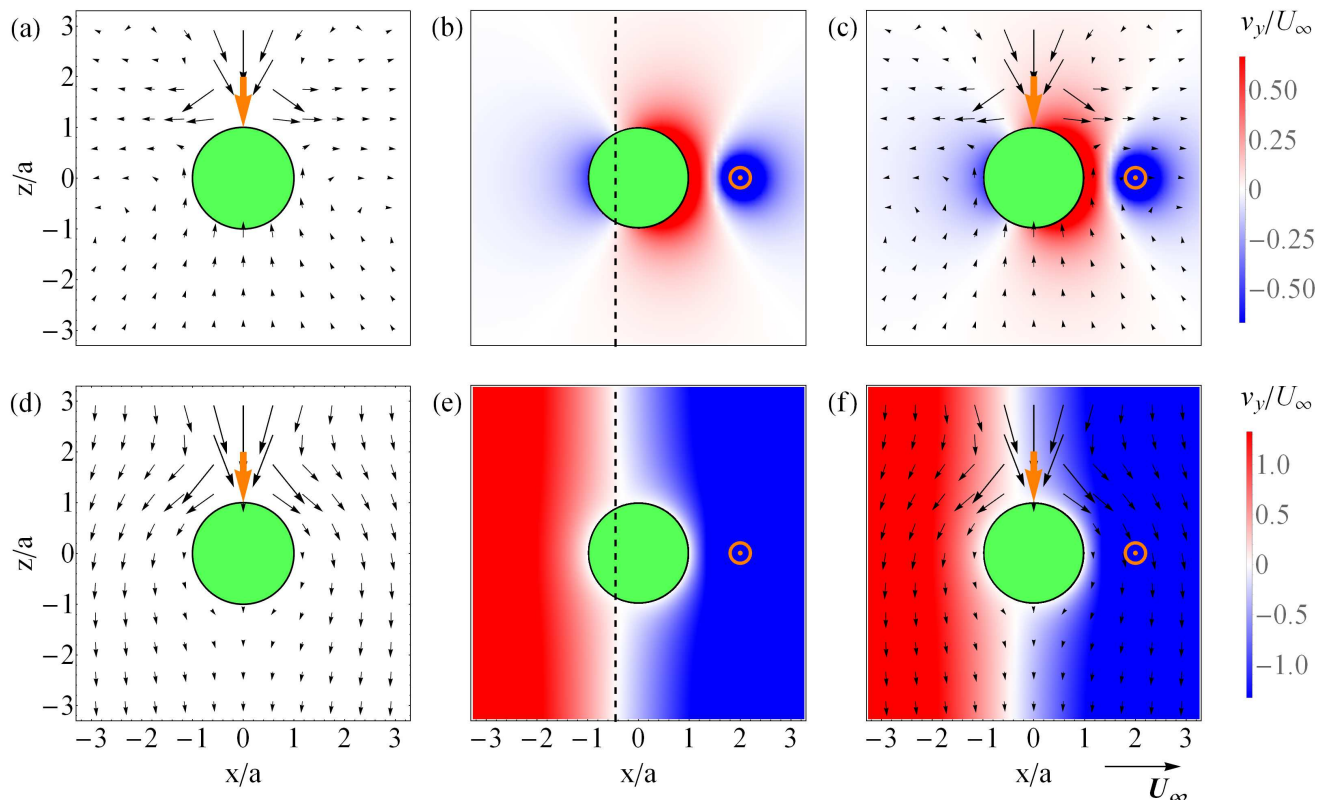
Figure 7. Flow fields for model microswimmer with straight, circular, and helical trajectories, respectively. (a)-(c) Laboratory frame of reference and (d)-(f) co-moving frame of reference. (a) and (d) Purely longitudinal flagellum, (b) and (e) purely transversal flagellum with the axis of rotation (dashed lines) indicated, and (c) and (f) both a longitudinal and a transversal flagellum of equal force magnitude $F_1 = F_2 = F$. Point forces (orange). The colour maps show the normalized out-of-plane component v_y/U_∞ with velocity scale $U_\infty = \sqrt{2}\,F/(6\,\pi\,\mu\,a)$.

[Nielsen and Kiørboe, 2015]. The clearance rate, i.e., the volume flow rate into the capture zone surrounding the cell should be calculated in the co-moving frame of reference in which the cell is at rest. With only the longitudinal flagellum active, the flagellate swims on a straight line and the model reduces to the previously studied model of copepods and uniflagellates (figures 7(a) and 7(d)) [Jiang et al., 2002, Langlois et al., 2009]. The flagellum enhances the flow velocities near the forward half of the cell surface, and it thereby increases the clearance rate for direct capture on the cell relative to the clearance rate for a towed sphere. The closer the point force is to the cell, the larger is the enhancement of the clearance rate [Langlois et al., 2009]. The transversal flagellum results in rotational flows with high velocities relative to the cell surface, in particular in the region nearest to the point force (figures 7(e) and 7(f)). However, the clearance rate in the region will presumably only be enhanced for the microswimmer with helical trajectory due to prey depletion in the water around the microswimmer with circular trajectory that retraces its path.

6. Conclusions

We have described an analytical model framework based on the exact solution of the creeping flow due to a point force next to a no-slip sphere, and we have illustrated how the model can be used to predict swimming kinematics and near-cell flows of flagellates with different flagellar arrangements and beat patterns. We believe that the model can be useful as a basis for the investigation of swimming velocities, search strategies, flow disturbances, feeding, and energy consumption. Thereby the model can contribute to the trait-based approach to aquatic ecology by providing a framework to investigate the flagellar arrangement as a key trait based on which optima and compromises between essential functions can be explored.

Acknowledgements

Appendix A. The flow due to a point force external to a sphere

Oseen's solution [Oseen, 1927, pp. 108] and [Higdon, 1979b, equations (3) and (4)] for the creeping flow due to a point force $\mathbf{F}$ next to a no-slip sphere with radius a is represented by a Green's function G_{jk} which depends on the field vector $\mathbf{x}$ with $r = |\mathbf{x}|$, and the positions $\mathbf{X}$ and $\mathbf{X}^* = (a^2/|\mathbf{X}|^2)\,\mathbf{X}$ of the point force and the inverse point:

$$
\begin{aligned}
G_{jk} =\ & \frac{\delta_{jk}}{|\mathbf{x}-\mathbf{X}|} + \frac{(x_j - X_j)(x_k - X_k)}{|\mathbf{x}-\mathbf{X}|^3} - \frac{a}{|\mathbf{X}|}\frac{\delta_{jk}}{|\mathbf{x}-\mathbf{X}^*|} \\
& - \frac{a^3}{|\mathbf{X}|^3}\frac{\left(x_j - X_j^*\right)\left(x_k - X_k^*\right)}{|\mathbf{x}-\mathbf{X}^*|^3} - \frac{|\mathbf{X}|^2 - a^2}{|\mathbf{X}|}\left\{ \frac{X_j^* X_k^*}{a^3\,|\mathbf{x}-\mathbf{X}^*|} \right. \\
& - \frac{a}{|\mathbf{X}|^2\,|\mathbf{x}-\mathbf{X}^*|^3}\left[X_j^*\left(x_k - X_k^*\right) + X_k^*\left(x_j - X_j^*\right)\right] \\
& + \left. \frac{2X_j^* X_k^*}{a^3}\frac{X_l^*\left(x_l - X_l^*\right)}{|\mathbf{x}-\mathbf{X}^*|^3}\right\} - \left(r^2 - a^2\right)\frac{\partial \phi_k}{\partial x_j}
\end{aligned}
\tag{A.1}
$$

with

$$
\begin{aligned}
\frac{\partial \phi_k}{\partial x_j} =\ & \frac{|\mathbf{X}|^2 - a^2}{2\,|\mathbf{X}|^3}\left\{ \frac{-3X_k\left(x_j - X_j^*\right)}{a\,|\mathbf{x}-\mathbf{X}^*|^3} + \frac{a\delta_{jk}}{|\mathbf{x}-\mathbf{X}^*|^3}\right. \\
& - \frac{3a\left(x_j - X_j^*\right)\left(x_k - X_k^*\right)}{|\mathbf{x}-\mathbf{X}^*|^5} - \frac{2X_k X_j^*}{a\,|\mathbf{x}-\mathbf{X}^*|^3} \\
& + \frac{6X_k}{a\,|\mathbf{x}-\mathbf{X}^*|^5}\left(x_j - X_j^*\right)\left(x_l - X_l^*\right)X_l^* \\
& + \left. \frac{3a}{|\mathbf{X}^*|}\frac{X_k^*\left(x_j - X_j^*\right)|\mathbf{x}-\mathbf{X}^*|^2 + \left(x_j - X_j^*\right)\left(x_k - X_k^*\right)|\mathbf{X}^*|^2}{|\mathbf{x}-\mathbf{X}^*|^3\,|\mathbf{X}^*|\left(|\mathbf{X}^*|\,|\mathbf{x}-\mathbf{X}^*| + x_l X_l^* - |\mathbf{X}^*|^2\right)}\right.
\end{aligned}
$$

$$+ \frac{3a}{|\mathbf{X}^*|} \frac{\left(|\mathbf{x} - \mathbf{X}^*| - |\mathbf{X}^*|\right)|\mathbf{x} - \mathbf{X}^*|^2 |\mathbf{X}^*| \delta_{jk}}{|\mathbf{x} - \mathbf{X}^*|^3 |\mathbf{X}^*| \left(|\mathbf{X}^*| |\mathbf{x} - \mathbf{X}^*| + x_l X_l^* - |\mathbf{X}^*|^2\right)}$$

$$- \frac{3a}{|\mathbf{X}^*|} \frac{|\mathbf{X}^*| \left(x_j - X_j^*\right) + |\mathbf{x} - \mathbf{X}^*| X_j^*}{|\mathbf{x} - \mathbf{X}^*|^2 |\mathbf{X}^*| \left(|\mathbf{X}^*| |\mathbf{x} - \mathbf{X}^*| + x_l X_l^* - |\mathbf{X}^*|^2\right)^2}$$

$$\times \left(X_k^* |\mathbf{x} - \mathbf{X}^*|^2 - (x_k - X_k^*) |\mathbf{X}^*|^2 + (x_k - 2X_k^*) |\mathbf{x} - \mathbf{X}^*| |\mathbf{X}^*|\right)$$

$$- \frac{3a}{|\mathbf{X}^*|} \frac{x_j X_k^* + r |\mathbf{X}^*| \delta_{jk}}{r |\mathbf{X}^*| \left(r |\mathbf{X}^*| + x_l X_l^*\right)}$$

$$+ \frac{3a}{|\mathbf{X}^*|} \frac{\left(|\mathbf{X}^*| x_j + r X_j^*\right)\left(|\mathbf{X}^*| x_k + r X_k^*\right)}{r |\mathbf{X}^*| \left(r |\mathbf{X}^*| + x_l X_l^*\right)^2} \Bigg\} . \tag{A.2}$$

References

[Andersen et al., 2015] Andersen, A., Wadhwa, N., and Kiørboe, T. (2015). Quiet swimming at low Reynolds number. *Phys. Rev. E*, 91:042712.

[Berg, 2008] Berg, H. C. (2008). *E. coli in Motion*. Springer.

[Blake, 1971] Blake, J. R. (1971). A spherical envelope approach to ciliary propulsion. *J. Fluid Mech.*, 46:199–208.

[Crenshaw, 1993a] Crenshaw, H. C. (1993a). Orientation by helical motion - I. Kinematics of the helical motion of organisms with up to six degrees of freedom. *Bull. Math. Biol.*, 55:197–212.

[Crenshaw, 1993b] Crenshaw, H. C. (1993b). Orientation by helical motion - III. Microorganisms can orient to stimuli by changing the direction of their rotational velocity. *Bull. Math. Biol.*, 55:231–255.

[Crenshaw, 1996] Crenshaw, H. C. (1996). A new look at locomotion in microorganisms: Rotating and translating. *Amer. Zool.*, 36:608–618.

[Dölger et al., 2017] Dölger, J., Nielsen, L. T., Kiørboe, T., and Andersen, A. (2017). Swimming and feeding of mixotrophic biflagellates. *Sci. Rep.*, 7:39892.

[Drescher et al., 2011] Drescher, K., Dunkel, J., Cisneros, L. H., Ganguly, S., and Goldstein, R. E. (2011). Fluid dynamics and noise in bacterial cell-cell and cell-surface scattering. *Proc. Natl. Acad. Sci.*, 108:10940–10945.

[Drescher et al., 2010] Drescher, K., Goldstein, R. E., Michel, N., Polin, M., and Tuval, I. (2010). Direct measurement of the flow field around swimming microorganisms. *Phys. Rev. Lett.*, 105:168101.

[Fenchel, 1986] Fenchel, T. (1986). The Ecology of Heterotrophic Microflagellates. In Marshall, K. C., editor, *Advances in Microbial Ecology*, volume 9, chapter 2, pages 57–97. Springer, New York.

[Fenchel, 2001] Fenchel, T. (2001). How dinoflagellates swim. *Protist*, 152:329–338.

[Friedrich and Jülicher, 2009] Friedrich, B. M. and Jülicher, F. (2009). Steering chiral swimmers along noisy helical paths. *Phys. Rev. Lett.*, 103:068102.

[Friedrich and Jülicher, 2012] Friedrich, B. M. and Jülicher, F. (2012). Flagellar synchronization independent of hydrodynamic interactions. *Phys. Rev. Lett.*, 109:138102.

[Gibbons, 1981] Gibbons, I. R. (1981). Cilia and flagella of eukaryotes. *J. Cell Biol.*, 19:107s–124s.

[Goldstein, 2015] Goldstein, R. E. (2015). Green algae as model organisms for biological fluid dynamics. *Annu. Rev. Fluid Mech.*, 47:343–75.

[Guasto et al., 2012] Guasto, J. S., Rusconi, R., and Stocker, R. (2012). Fluid mechanics of planktonic microorganisms. *Annu. Rev. Fluid Mech.*, 44:373–400.

[Gurarie et al., 2011] Gurarie, E., Grünbaum, D., and Nishizaki, M. T. (2011). Estimating 3D movements from 2D observations using a continuous model of helical swimming. *Bull. Math. Biol.*, 73:1358–1377.

[Higdon, 1979a] Higdon, J. J. L. (1979a). The generation of feeding currents by flagellar motion. *J. Fluid Mech.*, 94:305–330.

[Higdon, 1979b] Higdon, J. J. L. (1979b). A hydrodynamic analysis of flagellar propulsion. *J. Fluid Mech.*, 90:685–711.

[Inouye and Hori, 1991] Inouye, I. and Hori, T. (1991). High-speed video analysis of the flagellar beat and swimming patterns of algae: possible evolutionary trends in green algae. *Protoplasma*, 164:54–69.

[Jennings, 1901] Jennings, H. S. (1901). On the significance of the spiral swimming of organisms. *Am. Nat.*, 35:369–378.

[Jennings, 1904] Jennings, H. S. (1904). *Contributions to the Study of the Behaviour of Lower Organisms.* Carnegie Institute of Washington Publication.

[Jiang et al., 2002] Jiang, H., Osborn, T. R., and Meneveau, C. (2002). The flow field around a freely swimming copepod in steady motion. Part I: Theoretical analysis. *J. Plankton Res.*, 24:167–189.

[Kiørboe, 2016] Kiørboe, T. (2016). Fluid dynamic constraints on resource acquisition in small pelagic organisms. *Eur. Phys. J. Special Topics*, 225:669–683.

[Kiørboe et al., 2014] Kiørboe, T., Jiang, H., Gonçalves, R. J., Nielsen, L. T., and Wadhwa, N. (2014). Flow disturbances generated by feeding and swimming zooplankton. *Proc. Natl. Acad. Sci.*, 111:11738–11743.

[Kurtuldu et al., 2013] Kurtuldu, H., Tam, D., Hosoi, A. E., Johnson, K. A., and Gollub, J. P. (2013). Flagellar waveform dynamics of freely swimming algal cells. *Phys. Rev. E*, 88:013015.

[Langlois et al., 2009] Langlois, V. J., Andersen, A., Bohr, T., Visser, A. W., and Kiørboe, T. (2009). Significance of swimming and feeding currents for nutrient uptake in osmotrophic and interception-feeding flagellates. *Aquat. Microb. Ecol.*, 54:35–44.

[Lauga, 2016] Lauga, E. (2016). Bacterial Hydrodynamics. *Annu. Rev. Fluid Mech.*, 48:105–130.

[Lauga and Powers, 2009] Lauga, E. and Powers, T. R. (2009). The hydrodynamics of swimming microorganisms. *Rep. Prog. Phys.*, 72:096601(36 pp).

[Lighthill, 1952] Lighthill, J. (1952). On the squirming motion of nearly spherical deformable bodies through liquids at very small Reynolds numbers. *Comm. Pure. Appl. Math.*, 5:109–118.

[Lighthill, 1976] Lighthill, J. (1976). Flagellar hydrodynamics. *SIAM Rev.*, 18:161–230.

[Nielsen and Kiørboe, 2015] Nielsen, L. T. and Kiørboe, T. (2015). Feeding currents facilitate a mixotrophic way of life. *ISME J.*, 9:2117–2127.

[Oseen, 1927] Oseen, C. W. (1927). *Neuere Methoden und Ergebnisse in der Hydrodynamik.* Akademische Verlagsgesellschaft Leipzig.

[Pak and Lauga, 2016] Pak, O. S. and Lauga, E. (2016). Theoretical Models of Low-Reynolds-Number Locomotion. In Duprat, C. and Stone, H. A., editors, *Fluid-Structure Interactions in Low-Reynolds-Number Flows*, chapter 4. Royal Society of Chemistry.

[Pécseli et al., 2014] Pécseli, H. L., Trulsen, J. K., and Fiksen, Ø. (2014). Predator-prey encounter and capture rates in turbulent environments. *Limnology and Oceanography: Fluids and Environments*, 4:85–105.

[Polotzek and Friedrich, 2013] Polotzek, K. and Friedrich, B. M. (2013). A three-sphere swimmer for flagellar synchronization. *New J. Phys.*, 15:045005.

[Pozrikidis, 1992] Pozrikidis, C. (1992). *Boundary Integral and Singularity Methods for Linearized Viscous Flow.* Cambridge University Press.

[Purcell, 1977] Purcell, E. M. (1977). Life at low Reynolds number. *Am. J. Phys.*, 45:3–11.

[Sleigh, 1981] Sleigh, M. A. (1981). Flagellar beat patterns and their possible evolution. *BioSystems*, 14:423–431.

[Stone and Duprat, 2016] Stone, H. A. and Duprat, C. (2016). Low-Reynolds-Number Flows. In Duprat, C. and Stone, H. A., editors, *Fluid-Structure Interactions in Low-Reynolds-Number Flows*, chapter 2. Royal Society of Chemistry.

[Wrobel et al., 2016] Wrobel, J. K., Cortez, R., Varela, D., and Fauci, L. (2016). Regularized image system for Stokes flow outside a solid sphere. *J. Comput. Phys.*, 317:165–184.